Persistent expression of microRNA-125a targets is required to induce murine hematopoietic stem cell repopulating activity

Luinenburg, Danielle G.; Dinitzen, Alexander Bak; Svendsen, Arthur Flohr; Cengiz, Roza; Ausema, Albertina; Weersing, Ellen; Bystrykh, Leonid; de Haan, Gerald

Published in:
Experimental Hematology

DOI:
10.1016/j.exphem.2020.12.002

Publication date:
2021

Experimental Hematology

Experimental Hematology 2021;94:47–59

Persistent expression of microRNA-125a targets is required to induce murine hematopoietic stem cell repopulating activity

Daniëlle G. Luinenburg, Alexander Bak Dinitzen, Arthur Flohr Svendsen, Roza Cengiz, Albertina Ausema, Ellen Weersing, Leonid Bystrykh, and Gerald de Haan

European Research Institute for the Biology of Ageing, University Medical Center Groningen, University of Groningen, Groningen, The Netherlands

(Received 17 September 2020; revised 10 December 2020; accepted 11 December 2020)

MicroRNAs (miRs) are small noncoding RNAs that regulate gene expression posttranscriptionally by binding to the 3′ untranslated regions of their target mRNAs. The evolutionarily conserved microRNA-125a (miR-125a) is highly expressed in both murine and human hematopoietic stem cells (HSCs), and previous studies have found that miR-125 strongly enhances self-renewal of HSCs and progenitors. In this study we explored whether temporary overexpression of miR-125a would be sufficient to permanently increase HSC self-renewal or, rather, whether persistent overexpression of miR-125a is required. We used three complementary in vivo approaches to reversibly enforce expression of miR-125a in murine HSCs. Additionally, we interrogated the underlying molecular mechanisms responsible for the functional changes that occur in HSCs on overexpression of miR-125a. Our data indicate that continuous expression of miR-125a is required to enhance HSC activity. Our molecular analysis confirms changes in pathways that explain the characteristics of miR-125a overexpressing HSCs. Moreover, it provides several novel putative miR-125a targets, but also highlights the complex molecular changes that collectively lead to enhanced HSC function.

Hematopoietic stem cells (HSCs) are responsible for the lifelong reconstitution of all mature blood cells. As differentiation of these cells is nonreversible and terminal, the balance between self-renewal and differentiation of HSCs is tightly regulated to ensure proper tissue function. Proper HSC function is regulated both extrinsically by environmental factors that are secreted by the supporting cells in the bone marrow known as the stem cell niche and intrinsically by stem cell intrinsic programs. One of these cell intrinsic regulatory components that control HSC function is microRNAs (miRs) [1,2]. These ~22-nucleotide-long noncoding RNAs are integrated into RNA-induced silencing complexes (RISCs) that mediate the interaction between miRs and their target mRNAs. After this interaction, the translation of mRNA into protein cannot be completed.

MicroRNA-125a is highly expressed in HSCs, and its expression declines on differentiation into more mature cell types further down the hematopoietic lineage [3]. MiR-125a is part of an evolutionarily conserved cluster, which also encodes miR-99b and let-7e. The miR-125 family consists of three paralogs (125a, 125b1, and 125b2) and has an important function in the regulation of the output and persistence of HSCs [1,4]. Mir-125b1 and mir-125b2 do not differ in sequence but are encoded by two separate loci. All three members of the miR-125 family have similar effects on HSCs when overexpressed [5]. Because of the high evolutionary conservation, all mature miR-125 family members are present in organisms ranging from nematodes to mammals [6] and have the same seed sequence in both mouse and human. We will refer to miR-125 as including all three or any of those family isoforms.

ABD is responsible for the experiments that led to Figure 2B and C. AFS helped with the experimental setup of the RNA sequencing experiment and bioinformatic data analysis. RC executed the experiments that led to Figure 1B and D.

Offprint requests to: Gerald de Haan, Laboratory of Ageing Biology and Stem Cells, European Research Institute for the Biology of Ageing, University Medical Centre Groningen, University of Groningen, Antonius Deusinglaan 1, 9700 AV Groningen, The Netherlands.; E-mail: g.de.haan@umcg.nl

Supplementary material associated with this article can be found in the online version at https://doi.org/10.1016/j.exphem.2020.12.002.

https://doi.org/10.1016/j.exphem.2020.12.002

Collectively, studies from multiple laboratories have convincingly demonstrated the unique ability of miR-125 to regulate HSCs [1,3,5,7,8]. On ectopic overexpression of miR-125a, the self-renewal capacity of HSCs is increased in both murine and human cells [8]. Remarkably, mir-125a is also able to confer on committed progenitors long-term repopulating ability, which they normally lack [7]. Using cellular barcoding, we recently found that mir125a is able to extend the longevity of HSC clones [8].

MiR-125 affects the activity of targets that need to be repressed to ensure HSC self-renewal and engraftment. However, remains unclear whether the continuous activity of miR-125 is required or whether temporary overexpression of miR-125 in HSCs is sufficient to induce their long-term self-renewal. In this study, therefore, we used a reversible expression system (in three different setups) to assess to what extent temporary activation of miR-125a is sufficient to increase the potential of HSCs. We show that reversal of miR-125a overexpression reverts HSCs back to their normal state. Thus, continuous expression of miR-125a is needed to induce self-renewing HSC activity. In addition to functional assays, we have performed transcriptome analysis of HSPCs in which miR-125a is overexpressed. We identify molecular pathways that explain the phenotype that is induced on miR-125a overexpression and identify novel HSC-specific miR-125a-associated gene expression changes.

Methods

Mice

Female C57BL/6.SJL (B6.SJL, CD45.1) donor mice were bred at the Central Animal Facility of the University of Groningen. Female C57BL/6 (B6, CD45.2) recipient mice were purchased from Envigo (Horst, The Netherlands) and housed under clean conventional conditions. All animal experiments were approved by the Groningen University Animal Care and Use Committee.

Retroviral transduction

Cells were prestimulated for 24 hours in StemSpan (Stemcell Technologies, Vancouver, BC, Canada) supplemented with 10% fetal calf serum (FCS), 1% penicillin–streptomycin, and a cytokine mix: stem cell factor (SCF, 300 ng/mL), Flt3 ligand (1 ng/mL), and interleukin (IL)-11 (20 ng/mL). Viral supernatant was produced by transfecting the Platinum-Eco cell line with Fugene HD Transfection Reagent (Promega, Madison, WI) according to the manufacturer's protocol and harvesting fresh virus 48 hours after transfection. Viral particles were bound to RetroNectin (Clontech, Kyoto, Japan)-coated plates according to the manufacturer's protocol. After prestimulation, HSCs were harvested, added to the virus-coated plates, and spun down at room temperature at 400*g* for 45 min to promote binding of the cells to the virus-coated plate.

Primary transplants

Donor cells were harvested from C57BL6/SJL (CD45.1) mice and sorted by fluorescence-activated cell sorting (FACS) for the LSK/SLAM (lineage$^-$Sca1$^+$cKit$^+$CD48$^-$CD150$^+$) phenotype. Recipient mice (B6, CD45.2) were conditioned with a lethal dose (9 Gy) of total-body irradiation. Transduced cells were transplanted at different dosages in the presence of 2 million supporting cells from a cKit-deficient (W41) donor by retro-orbital injection. Ciprofloxacin was added to the drinking water of recipient mice for 10 days, starting 1 day before irradiation. Donor engraftment was tracked by performing retro-orbital peripheral blood sampling every 4 weeks. Erythrocytes were lysed with ammonium chloride-based lysis buffer, and remaining white blood cells were stained for CD45.1/2 and the markers Mac-1/Gr-1, B220 and CD3. Both stem cell and peripheral blood staining protocols are described in the Supplementary Data (online only, available at www.exphem.org).

Serial transplants

Donor cells were harvested from primary/secondary recipients from the miR-125a overexpression and control groups. Total bone marrow was stained for the LSK/SLAM (lineage$^-$Sca1$^+$cKit$^+$CD48$^-$CD150$^+$) markers for analysis; however, sorting was only performed based on the lineage and Sca1 markers (Supplementary Figure E1, online only, available at www.exphem.org). We have previously described how cKit is a target of miR-125a, resulting in unreliable expression of this stem cell marker in 125a-overexpressing cells [8]. Sorted lineage$^-$Sca1$^+$GFP$^+$ were transduced with the self-inactivating Cre plasmid [9] according to the described transduction protocol and either transplanted directly into secondary recipients or subjected to in vitro expansion. Separation of GFP$^+$ and mCherry$^+$ stem cells took place by sorting bone marrow from secondary recipients or in vitro expansion (Supplementary Figure E2, online only, available at www.exphem.org). GFP$^+$ and mCherry$^+$ cells originating from the same bone marrow sample were transplanted in equal doses to ensure comparability.

Cre-loxP system

The MXW-pPGK- IRES-eGFP retroviral vector used for overexpression of miR-125a was constructed as previously described [3,5]. The first LoxP sequence was inserted directly after the pPGK promotor region using the *Xho*I and *Eco*RI restriction sites (oligo sequences: [+] TCGAG ataacttcgtatagcatacattatacgaagttatGTATGG, [−] AATTCCATACataacttcgtataatgtatgctatacgaagttatC). The second LoxP sequence was inserted behind IRES-eGFP using the *Sal*I and *Not*I restriction sites (oligo sequences: [+] GGCCGCataacttcgtatagcatacattatacgaagttatAGATAG, [−] TCGACTATCT ataacttcgtataatgtatgctatacgaagttatGC). Finally, the mCherry sequence was amplified from a donor vector (pLM-CMV-R-Cre) with primers that included a STOP codon insertion, and inserted behind the second LoxP site (forward: TAAGCAGTCGACatggtgagcaagggcgagga; reverse: tgcttaGTCGACTTA cttgtacagctcgtccatgccg). This resulted in a plasmid that contains the miR-125a genomic sequence linked to IRES-eGFP flanked by two LoxP sites (floxed) followed by mCherry (Figure 1A). The LoxP sites allow for Cre-recombinase–mediated

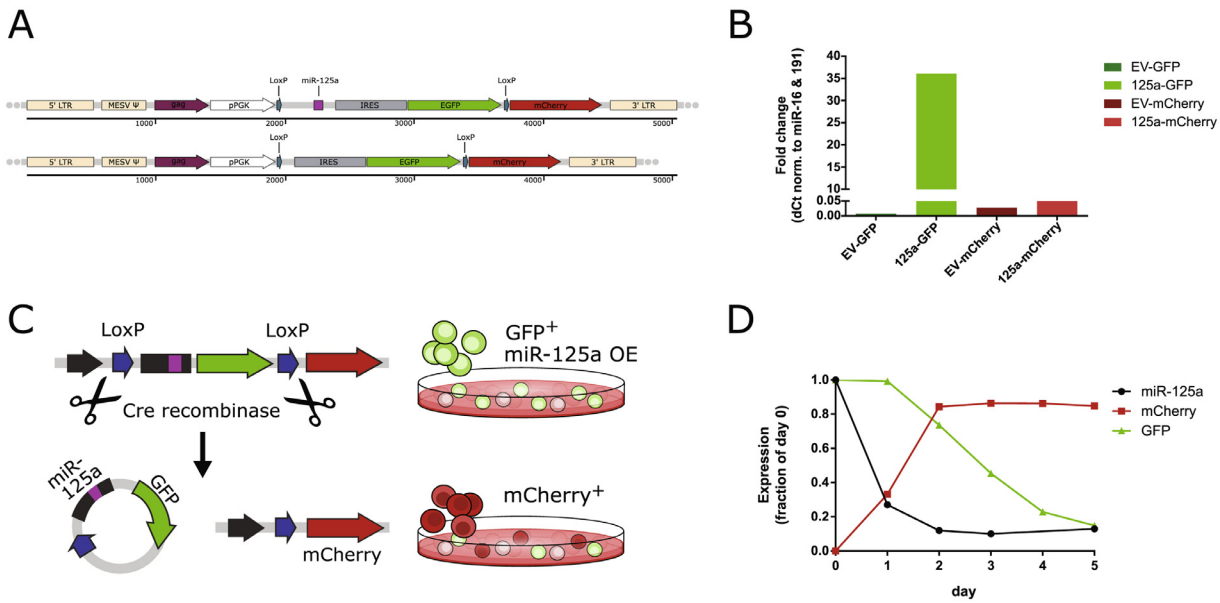

Figure 1. Setup and kinetics of Cre-LoxP reversible miR expression system. **(A)** Schematic representation of the retroviral plasmid, both for 125a OE and for the empty vector control. **(B)** Overview of reversal of overexpression by Cre recombinase, resulting in a switch of fluorescent proteins. **(C)** MiR-125a expression levels on overexpression and reversal in 32D cell line. **(D)** Kinetics of reversal. Change in expression expressed as fraction of expression on day 0. Fluorescence measured by flow cytometry, and miR-125a levels measured by RT-qPCR.

excision and, thus, shutdown of miR-125a overexpression, while at the same time switching the fluorescent tag from GFP to mCherry. Cre-recombinase expression is established by transducing the target cells with a self-inactivating Cre expression plasmid [9] according to the transduction protocol described above.

In vitro expansion of HSCs

Culture conditions described in Wilkinson et al. [10] were adapted to suit the needs of this experiment. The culture medium was Ham's F12 (Gibco, Invitrogen, Waltham, M) supplemented with 1% penicillin/streptomycin/glutamine (P/S/G), 10 mmol/L Hepes, 1 mg/mL polyvinyl alcohol (PVA), insulin −transferrin−selenium−ethanolamine (ITSX), plus cytokines: 10 ng/mL SCF and 100 ng/mL thrombopoietin (TPO). Cells were kept in RetroNectin-coated six-well plates as described for transduction. Cells were seeded at $0.5-1 \times 10^6$ cells/well, and daily 90% medium changes were performed to eliminate cell debris, metabolites, and inflammatory cytokines and ensure constant culture conditions.

Cobblestone assays

The cobblestone area-forming cell (CAFC) assay was performed as previously described [11–13]. In short, hematopoietic cells were seeded onto a feeder layer (FBMD-1) in 96-well plates in a limiting dilution fashion. Wells were scored positive or negative for formation of cobblestone areas and 50% of the medium was refreshed weekly. Early emerging colonies (days 7–14) were indicative of progenitor activity, and late emerging colonies (day >35) were indicative of activity of more quiescent stem cells. The Extreme Limiting Dilution Analysis (ELDA) tool from the Walter+Eliza Hall Institute of Medical Research [14] was used to estimate stem cell frequencies and test differences between the experimental groups.

RNA sequencing

Freshly isolated bone marrow (BM) lineage$^-$Sca1$^+$GFP$^+$ cells were sorted as illustrated in Supplementary Figure E2. Two thousand cells were directly sorted into polymerase chain reaction (PCR) tubes containing 6 μL NEBNext Cell Lysis Buffer supplemented with RNase inhibitor buffer, immediately frozen in dry ice, and stored at −80°C awaiting library prep. Library prep was performed according to the NEBNext single cell/low input RNA library prep kit for Illumina (New England Biolabs, Ipswich, MA) according to the manufacturer's protocol. Three control and three OE samples were pooled in equimolar fashion and sequenced on an Illumina NextSeq500 platform. De-multiplexed sequencing reads were subjected to quality control and mapped to the murine genome (version M21) with STAR aligner optimized for paired end reads of 50 bp. Differential expression analysis was performed using edgeR; in brief, low read counts were removed, and normalization method TMM was applied. One sample of each experimental group was removed. Furthermore, the glmQLFit/glmLRT model was used to fit the data. Differentially expressed genes were selected with the topTags function, using Benjamini −Hochberg adjustment and a significance threshold at $p < 0.05$. The data discussed in this publication have been deposited in NCBI's Gene Expression Omnibus [15] and are accessible through GEO Series Accession No. GSE158126 (https://www.ncbi.nlm.nih.gov/geo/query/acc.cgi?acc=GSE158126).

Results

We evaluated the effects of reversal of miR-125a overexpression on the functioning of HSCs using three

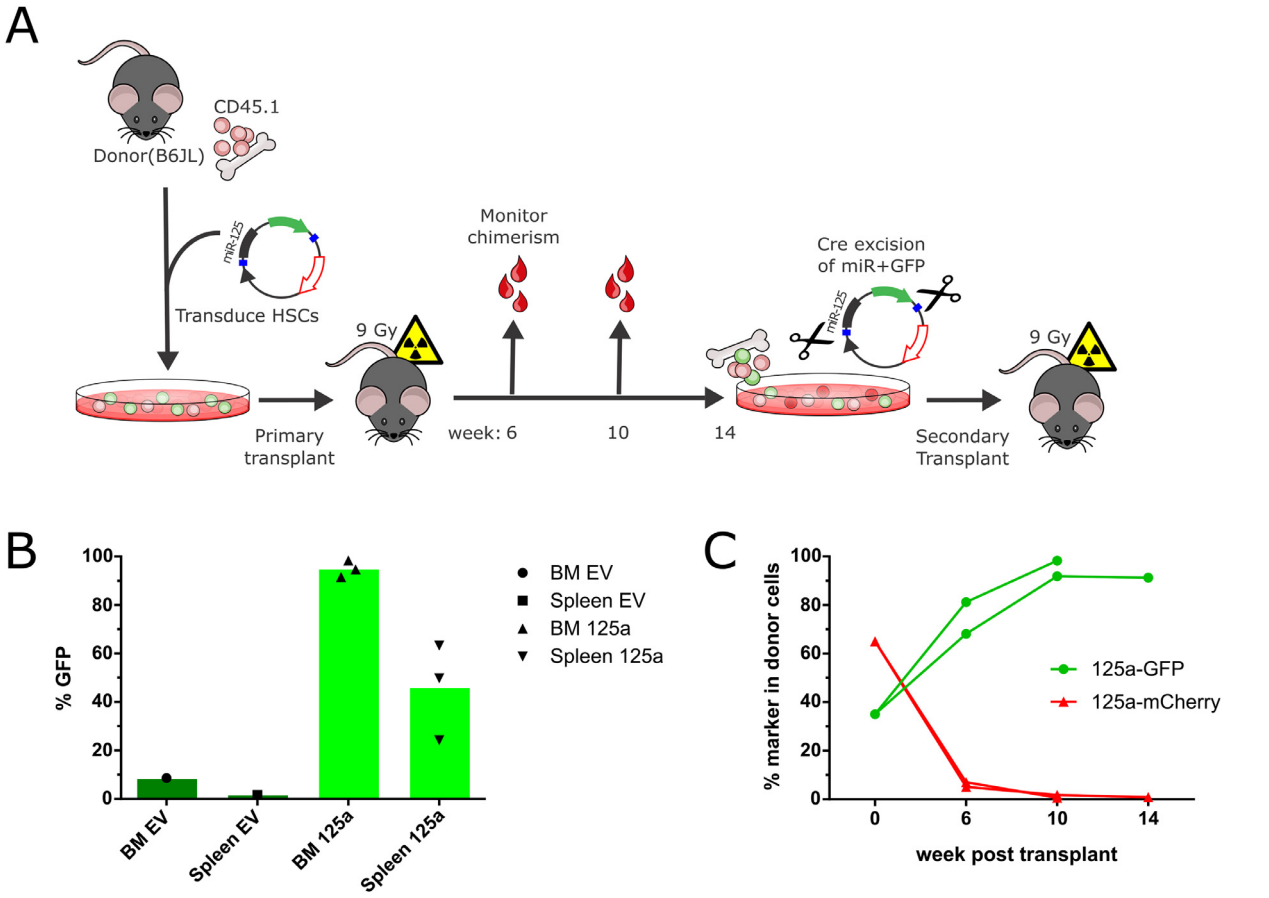

Figure 2. Continuous overexpression of miR-125a is necessary for the proliferative advantage phenotype. **(A)** Experimental setup. **(B)** Contribution of GFP^+ cells to the total white blood cell (WBC) population in bone marrow (BM) and spleen of mice transplanted with cells transduced with an empty vector (EV) or with miR-125a overexpression ($n = 3$ mice/group). **(C)** Contribution over time of $CD45.1^+GFP^+$ and $CD45.1^+mCherry^+$ cells to the peripheral blood of secondary recipients.

different in vivo approaches. First, we performed competitive transplantation studies in which miR-125a –overexpressing cells were transplanted alongside HSCs in which miR-125a overexpression was reversed (Figure 1). In a second set of experiments, we performed noncompetitive transplantations in which miR-125a reversed cells were transplanted into recipients without the competitive pressure of cells that still overexpressed miR-125a (Figure 2). Finally, we expanded HSCs in which miR-125a was overexpressed, then deleted in vitro, and compared their engraftment activity noncompetitively (Figure 3).

Using Cre-LoxP recombination to reverse miR-125a overexpression in hematopoietic cells

To investigate whether the potent effect of miR-125a on HSCs requires its constitutive expression, we used the Cre-LoxP system to generate a reversible overexpression system that allows tracking of cells in which miR-125a expression is induced and simultaneously labels cells in which miR-125a expression has been reversed. To this end we generated a retroviral vector, based on the vector previously used for 125a overexpression [5], and added LoxP palindromic sites and a second fluorescent marker (Figure 1A). This allows for Cre-recombinase–mediated reversal of miR expression accompanied by switching of a stably integrated fluorescent marker (Figure 1B). On miR-125a overexpression, cells are marked with green fluorescent protein (GFP); at any desired time, these cells can be reverted back to endogenous expression levels of miR-125a, which then simultaneously marks these reverted cells with mCherry (red fluorescent protein). The reversal of miR-125a expression to endogenous levels is apparent 48 hours after Cre-recombinase activation and is accompanied by expression of the red fluorescent protein mCherry (Figure 1C). FACS analysis indicates that the switch of fluorescent labels from GFP to mCherry requires 5 days to be fully completed (Figure 1D).

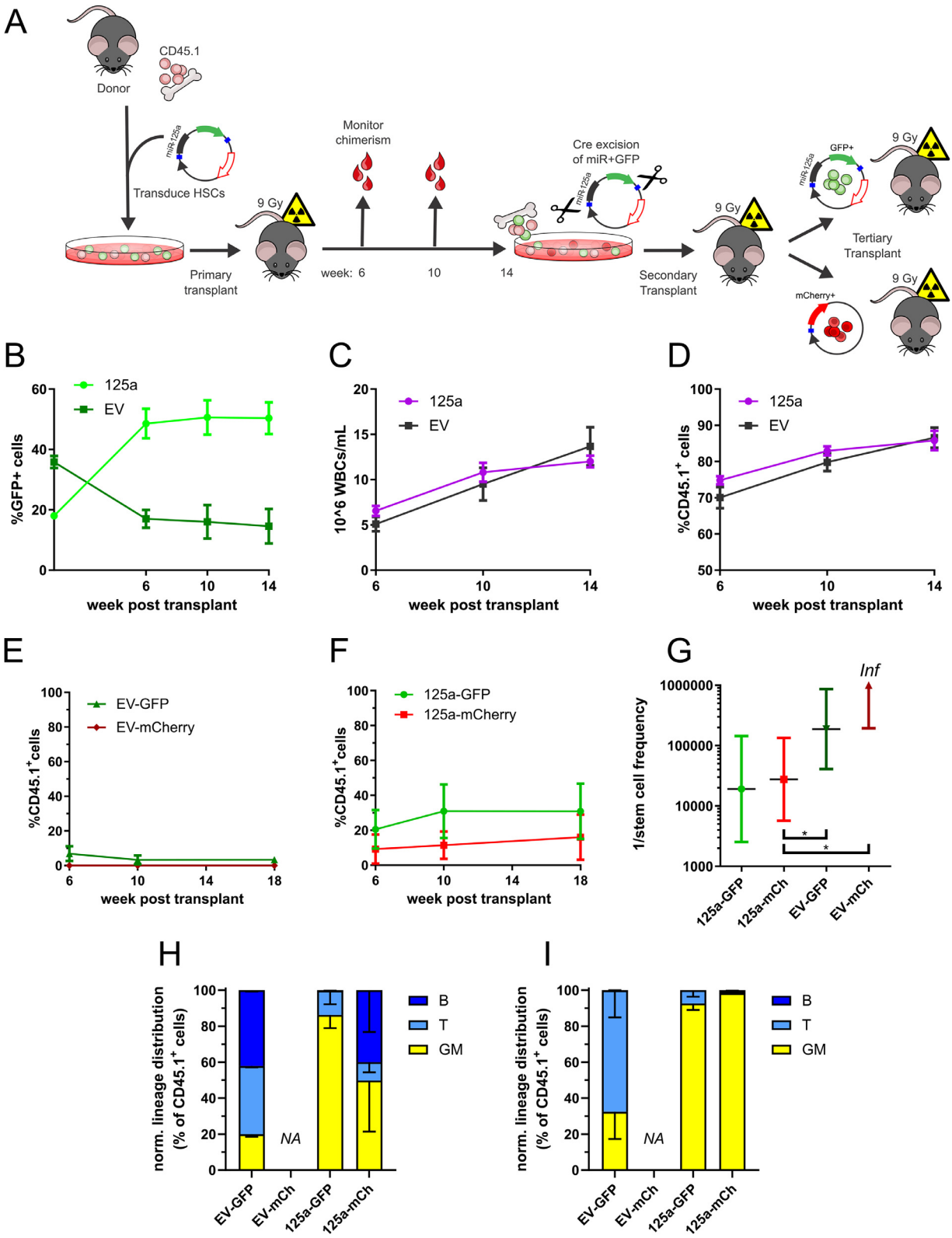

Figure 3. Reversed cells are still functional in noncompetitive transplant. **(A)** Experimental setup. **(B)** CD45.1$^+$GFP$^+$ cells in peripheral blood of primary recipients ($n = 6–8$ mice/group). **(C,D)** WBC counts and donor contribution (CD45.1$^+$) in peripheral blood of primary recipients ($n = 6–8$ mice/group). **(E,F)** Donor contribution of reversed cells to the peripheral blood in mice transplanted with EV control cells and miR-125a OE cells in tertiary transplants ($n = 4–6$ mice/group). **(G)** Estimated stem cell frequencies based on transplantation dose and engraftment of tertiary recipients, calculated with ELDA tool [14]. Recipients were marked as positive if >1% of the donor contribution was present in total living

Continuous overexpression of miR-125a is required to evoke the proliferative advantage of HSCs

By use of this reversible expression system, competitive serial transplants were performed to establish whether continuous expression of miR-125a is required to increase HSC potency (Figure 2A). Here we use the term *competition* to indicate the interplay between the two subpopulations in the donor pool: the miR-125a –overexpressing GFP$^+$ cells and the reversed mCherry$^+$ cells. The transplantation protocol included a lethal dose of irradiation and the use of W41 supporting cells, which provide short-term radioprotection but no long-term engraftment. First, donor cells were harvested from B6.SJL (CD45.1) mice, and miR-125a overexpression was induced by viral transduction of the reversible expression vector. HSCs were then transplanted into lethally irradiated B6 (CD45.2) recipients and allowed to engraft for 14 weeks. After 14 weeks, the bone marrow was harvested and, as expected, strong engraftment of the miR-125a–overexpressing cells was observed (Figure 2B). Reversal of miR-125a expression was subsequently induced in vitro using viral transduction of a self-inactivating Cre-recombinase expression vector, and cells were immediately transplanted competitively into secondary recipients. The contribution of GFP$^+$ and mCherry$^+$ cells to the peripheral blood was monitored at various intervals (Figure 2C). In such a competitive setup, reversed cells were outcompeted by miR-125a–overexpressing cells in 2 weeks.

MiR-125a reversion does not negatively affect HSC function

In the previous experiment, reversed and nonreversed cells were in competition with each other. It is clear that GFP$^+$ cells that still overexpress miR-125a outcompeted the reversed mCherry$^+$ cells. From that experiment it was not clear whether mCherry$^+$ cells were exhausted or whether these cells still possessed HSC potential but were outcompeted by the highly competent HSCs that were still overexpressing miR-125a. Thus, in an alternative approach, HSCs in which miR-125a overexpression was reverted were transplanted noncompetitively. This approach allowed assessment of their function without the potent competition of miR-125a–overexpressing cells (Figure 3A). Similar to the experiment described above and outlined in Figure 2A, cells were harvested from CD45.1$^+$ donor mice, transduced with the reversible expression vector, and transplanted into lethally irradiated CD45.2$^+$ primary recipients. The contribution of GFP$^+$ miR-125a –overexpressing cells (Figure 3B), total white blood cell counts (Figure 3C), and donor chimerism (Figure 3D) was measured in peripheral blood. After 14 weeks, bone marrow of the primary recipient was harvested, and reversal of miR-125a OE was induced by Cre-recombinase expression. Unfractionated cells were then immediately transplanted into a secondary recipient to ensure proper maturation of the fluorescent proteins. Bone marrow of the secondary recipients was harvested after 2 weeks, and GFP$^+$ and mCherry$^+$ were separated by FACS and noncompetitively transplanted in limiting dilution into tertiary recipients. In the tertiary recipients, the contribution to the peripheral blood was measured by total donor engraftment (Figure 3E, F), and stem cell frequencies were estimated based on transplantation dose and engraftment. Stem cell frequencies in both miR-125a–overexpressing and reversed cells were approximately tenfold higher compared with those in the empty vector control samples, and there were no significant differences between the miR-125a–overexpressing and reversed groups ($p = 0.056$) (Figure 3G). Progeny of miR-125a–overexpressing HSCs exhibited myeloid skewing, as reported previously[5,7], which is also visible in the peripheral blood of tertiary recipients at week 10 (Figure 3H) and week 18 (Figure 3I) posttransplant. Interestingly, this skewing of lineage distribution was persistent in the reverted mCherry$^+$ cells in the miR-125a group. These experiments revealed that after reversal of miR-125a overexpression, HSCs have a similar stem cell frequency and are still able to engraft and contribute to the peripheral blood.

Serial transplants induce significant proliferative stress on the transplanted HSCs. As an alternative approach to assess the effects of miR-125a reversibility, we eliminated secondary transplantations and instead used a recently described 6-day in vitro expansion protocol [10]. After in vitro culture, we again separated the GFP$^+$ cells from the mCherry$^+$ cells by FACS and assessed HSC function by CAFC assay and by transplantation (Figure 4A). After 6 days of in vitro expansion, cells were analyzed for expression of lineage and stem cell markers (Figure 4B,C). The cultured cells remained lineage negative and had similar LSK and LSK/SLAM phenotypes in the different experimental conditions. CAFC assays revealed that the miR-

cells of bone marrow. Data are expressed as 95% confidence interval of 1/(stem cell frequency). Pairwise differences tested by χ^2 test: statistically significant difference between 125a-mCherry and EV-GFP/EV-mCherry (p values, respectively, 0.0009 and 0.0013). **(H,I)** Lineage distribution expressed as a percentage of CD45.1$^+$ donor cells in peripheral blood of secondary recipients at week 10 (H) and week 18 (I) posttransplant. *GM*=granulocyte/macrophage (Gr1/Mac1); *T*=T cells (CD3); *B*=B cells (B220). Normalized to sum of lineage$^+$ cells (Gr1/Mac1/CD3/B220 positive) ($n = 2$ or 3 mice/group).

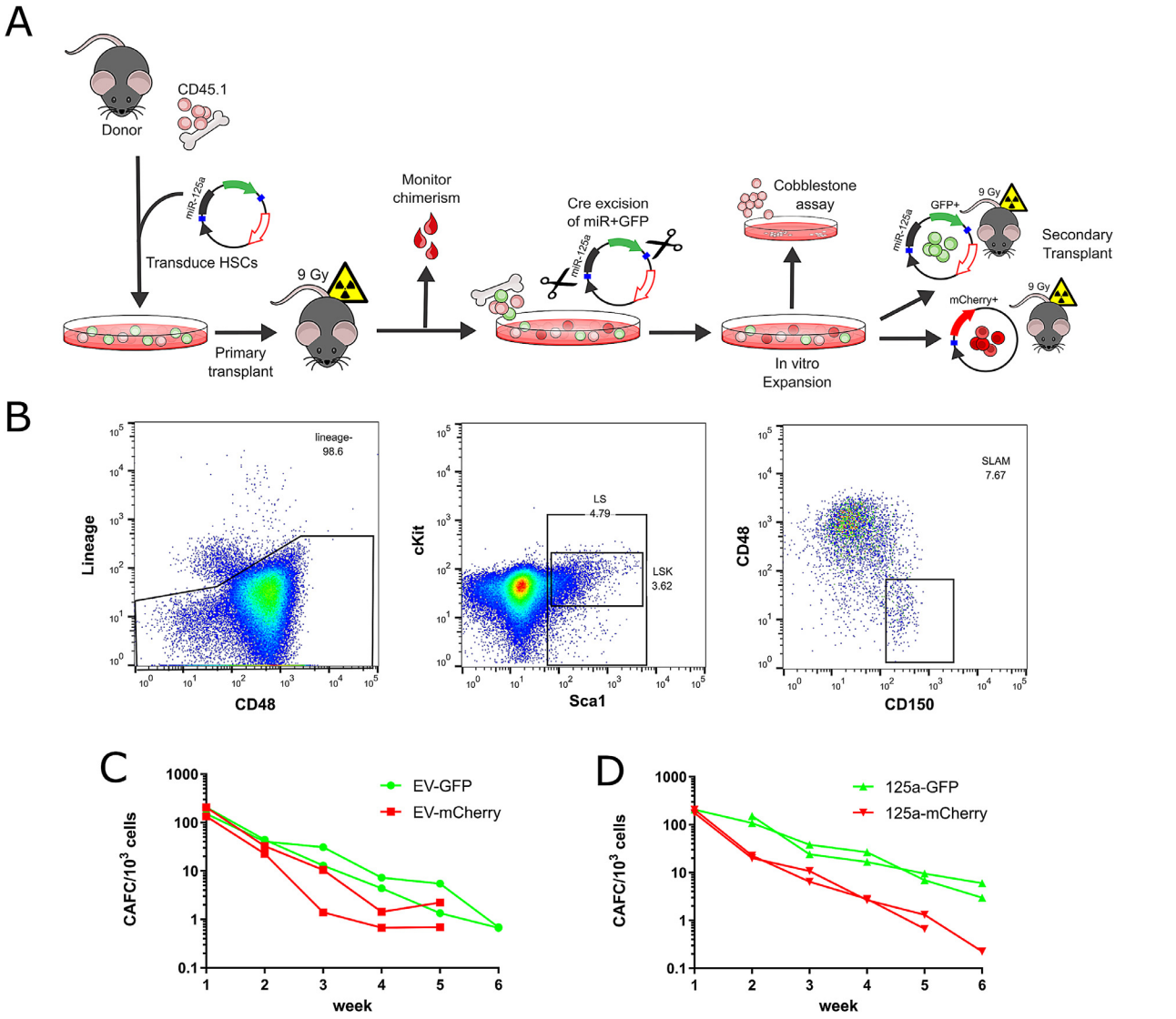

Figure 4. Reversed cells behave like normal stem cells in vitro. **(A)** Experimental setup. **(B)** Cell surface phenotype of lineage$^-$Sca1$^+$ cells exposed to 6 days of in vitro culture. Shown are the LSK and LSK/SLAM compartments. **(C,D)** Cobblestone area-forming cell frequency per 1,000 seeded cells shown per week after initiation for respectively EV and miR-125a OE cells.

125a–overexpressing GFP$^+$ cells maintained the highest frequency of late-appearing CAFCs. Within the EV control groups, no difference was observed between the GFP$^+$ and reversed mCherry$^+$ cells, as expected. At week 2, the average numbers of CAFCs/10^3 cells for EV-GFP, EV-mCherry, 125a-GFP, and 125a-mCherry were 3.40, 1.46, 8.23, and 0.99, respectively. At week 5, the average numbers of CAFCs/10^3 cells for EV-GFP, EV-mCherry, 125a-GFP, and 125a-mCherry were 42.4, 27.7, 130.6, and 21.3, respectively. Between the two replicates of the miR-125a groups, an average decrease in early-appearing progenitor colonies at week 2 (day 14) of approximately eightfold and an approximately sixfold decrease in late-appearing stem cell colonies at week 5 (day 35) were observed on reversal of miR-125a overexpression.

The various cell populations (HSCs that still overexpress mir125a, HSCs that expressed miR125a in primary recipients, and the empty vector control cells) were all transplanted noncompetitively into secondary recipients at different doses (Figure 5B). In these experiments 125a-GFP+ cells outperformed control cells, as well as 125a-mCherry cells that no longer overexpressed miR-125a, as indicated by a higher contribution of these cells to the peripheral blood of recipients over time (Figure 5A). At week 12 there is a clear difference in donor contribution to the peripheral blood (Figure 5C). On sacrifice at week 22

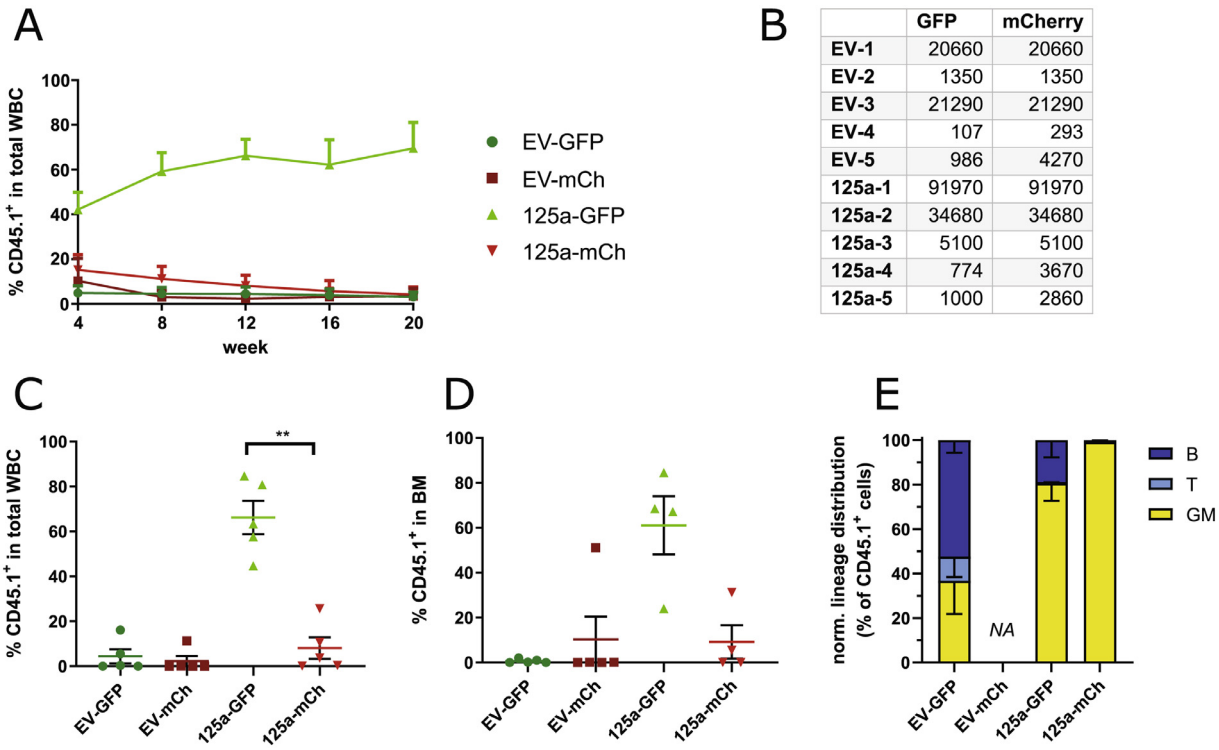

	GFP	mCherry
EV-1	20660	20660
EV-2	1350	1350
EV-3	21290	21290
EV-4	107	293
EV-5	986	4270
125a-1	91970	91970
125a-2	34680	34680
125a-3	5100	5100
125a-4	774	3670
125a-5	1000	2860

Figure 5. Donor contribution of in vitro expanded cells measured in the peripheral blood of secondary recipients. **(A)** Donor contribution (%CD45.1) of total white blood cells (WBC) ($n = 4$ or 5 mice/group). **(B)** Number of transplanted lin$^-$Sca1$^+$ cells. **(C)** Donor contribution (%CD45.1) in peripheral blood of individual recipients ($n = 5$) at week 12 posttransplant. Difference between 125a-GFP and 125a-mCherry tested by paired t test ($p = 0.0022$). **(D)** Donor contribution (%CD45.1) in bone marrow of secondary recipients at week 22 posttransplant. **(E)** Lineage distribution expressed as percentage of CD45.1$^+$ donor cells in bone marrow of secondary recipients at week 22 posttransplant. *GM*=granulocyte/macrophage (Gr1/Mac1); *T*=T cells (CD3); *B*=B-cells (B220). Normalized to sum of lineage$^+$ cells (Gr1/Mac1/CD3/B220 positive; $n = 2–4$ mice/group).

posttransplant, we measured engraftment in the bone marrow and found high chimerism levels in mice transplanted with mir-125–overexpressing cells. This indicates that HSCs that still overexpress miR-125a will outperform reversed and empty vector control cells (Figure 5D). In the bone marrow, the same lineage skewing was visible as seen in the peripheral blood in the previous experiment (Figure 3H,I). We observed skewing toward the myeloid lineage in the progeny of both miR-125a–overexpressing and reversed HSCs (Figure 5E).

Identification of microRNA-125a–associated transcripts by RNA sequencing

To provide insight into the molecular mechanisms by which miR-125a exerts its function, we established the transcriptome changes on expression of miR-125a using RNA sequencing. For this purpose, 2000 lineage$^-$Sca1$^+$GFP$^+$ 125a-overexpressing or EV control cells were isolated from primary recipients 12 weeks after transplantation. At this time, HSCs have had time to recover from the transplantation procedure and return to a steady state. Direct effects of miRs on their target mRNA could result in both a decrease and an increase in mRNA abundance. Potentially, a miR could also stabilize mRNA abundance, in which case we would not be able to identify these transcripts with this approach. Differential expression analysis revealed 156 downregulated and 237 upregulated genes. Comparison of differentially expressed genes with predicted miR-125a targets (compiled from four commonly used sources: PicTar, TargetScan, miRanda, and miRDB) allowed us to identify 12 predicted targets that were downregulated on miR125a overexpression, but we also identified 19 predicted miR-125a targets that were upregulated (Figure 6A,B).

Table 1 provides an overview of the 12 predicted miR-125a target genes that were significantly repressed in cells overexpressing miR-125a compared with empty vector control cells. The functional role of many of these putative miR-125a targets specifically in HSCs remains to be determined. However, the 2 miR-125a–predicted target genes that were most prominently affected, glutaminase (Gls) and Ras-related protein Rap-1A (Rap1a), have previously been reported to affect HSC function. Gls is a K-type mitochondrial

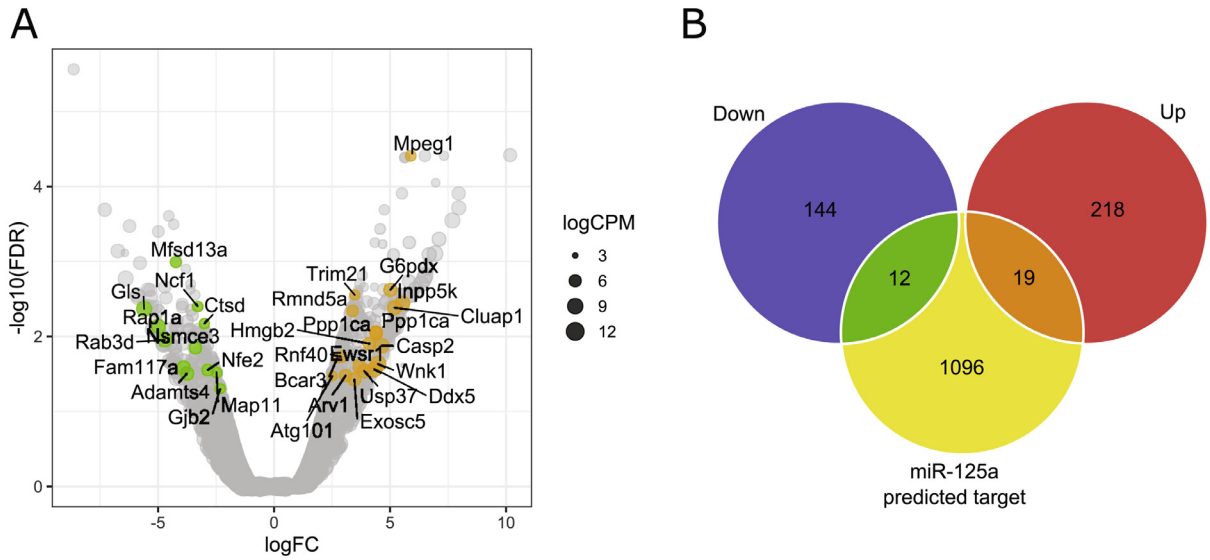

Figure 6. Identification of predicted targets of miR-125a by RNA sequencing. **(A)** Scatterplot of gene expression, revealing log fold change (log FC), −log false discovery rate (−log FDR) and expression levels expressed as the log count per million (log CPM). A predicted miR-125a target list was compiled from four commonly used databases: PicTar, TargetScan, miRanda, and miRDB. Genes occurring in both the compiled predicted miR-125a target list and significantly differentially expressed are annotated with their gene name, downregulated genes in green and upregulated genes in orange. **(B)** Overlap between the number of downregulated genes (Down), upregulated genes (Up), and compiled predicted miR-125a target list. Hypergeometric probability of overlap Down + Target $p = 0.10$, Up + Target $p = 0.067$, assuming a total population of 17,039, representing all annotated genes in DE table generated from RNA sequencing data.

glutaminase expressed by different transcript variants mediated by alternate splicing. In HSCs, it has very recently been found that the GLS protein is critical for the control of HSC self-renewal and that isoform switching of Gls is required for the activation of HSCs [16]. Whereas increased GLS levels maintain HSCs in a quiescent state, here we illustrate that miR-125a decreases GLS transcripts, which coincides with increased HSC proliferation.

Rap1a is a partner of podocalyxin (Podxl) and can be activated by erythropoietin (Epo) or IL-3. Rap1a is strongly activated when HSCs are challenged with granulocyte colony-stimulating factor (G-CSF) and can modulate cell migration and adhesion [17,18]. Previously, we established that miR-125a–overexpressing HSCs respond more strongly to G-CSF compared with control cells [8]. Other putative miR-125a targets that have previously been linked to lineage commitment are

Table 1. miR-125a–predicted targets that are significantly downregulated in HSPCs on miR-125a overexpression

Gene[a]	Log FC[b]	*p* Value[c]	Function HSC[d]	Other function[e]
Gls	−5.60	2.41×10^{-5}	Required for activation [16]	Glutamine metabolism [7]
Rap1a	−.98	5.38×10^{-5}	HSC maintenance [19]	Cell adhesion, migration
Rab3d	−4.71	0.000116	Unknown	Intracellular vesicle transport [20]
Mfsd13a (TMEM180)	−4.24	1.79×10^{-6}	Unknown	Transmembrane protein [21,22]
Fam117a	−3.89	0.000416	Unknown	C/EBP-induced protein
Adamts4	−3.75	0.000602	Unknown	Arthritis [23]
Nsmce3 (MAGEG1)	−3.38	0.000169	Unknown	DNA repair [24]
Ncf1	−3.30	1.89×10^{-5}	Unknown	NADPH oxidase component [25]
Ctsd	−3.01	4.86×10^{-5}	Lineage commitment [26]	Lysosomal protease
Nfe2	−2.86	0.000459	Erythroid/megakaryocytic lineage [27]	Transcription factor
Map11	−2.48	0.000538	Unknown	Associates with mitotic spindles [28]
Gjb2	−2.32	0.001171	Unknown	Gap junction protein

[a]Gene name, alias in parentheses.
[b]Fold change as determined by RNA sequencing.
[c]*p* value as calculated in RNA sequencing.
[d]Function in HSC or related to hematopoiesis.
[e]General function of protein.

the peptidase cathepsin D (Ctsd) and transcription factor nuclear factor erythroid 2 (Nfe2). The remaining transcripts that we identify as potential miR-125a targets in HSCs have no known function in the hematopoietic system.

Molecular signatures that are associated with miR-125a–enhanced HSC potential

Beyond the potential identification of miR-125a targets, we further explored the overall molecular pathways that were affected by miR-125a overexpression. Although these changes may be caused by both direct and indirect effects of miR-125a, they will aid in better understanding the phenotype that is observed in HSCs. We used the Molecular Signatures Database [29], to compare the 321 differentially expressed genes with different molecular signatures. Using this tool, we identified three molecular processes to be significantly enriched in this group of genes (Figure 7). The most strongly associated gene set contained transcripts involved in G2/M checkpoint control. This checkpoint prevents a cell from entering mitosis in the case of damaged DNA. Second, there was significant overlap between the differentially expressed genes on miR-125a overexpression and targets of c-Myc, a transcription factor associated with metabolic changes and cell proliferation [53]. Lastly, we identified overlap with E2F targets that regulate cell cycle and DNA synthesis. These three most strongly associated gene sets are all involved in cell proliferation, which is in line with the observed functional and phenotypical changes of miR-125a–overexpressing HSCs.

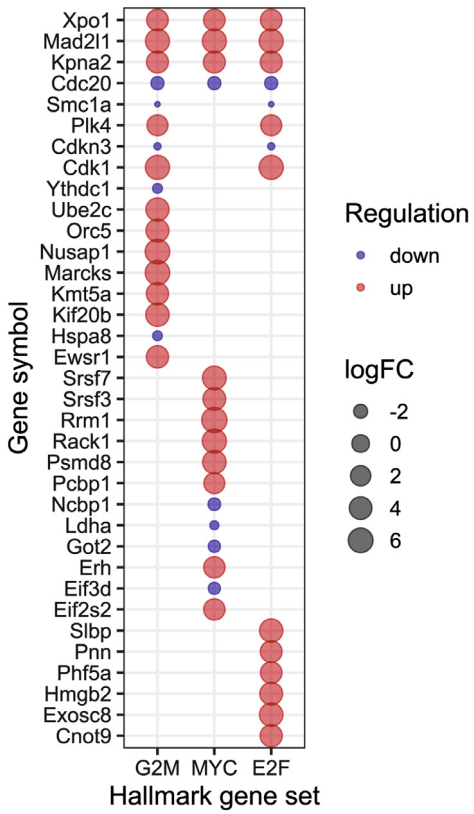

Figure 7. Top three enriched genes using all differentially expressed genes as input. The X indicates whether a differentially expressed gene is present in one or more of the following sets: G2/M checkpoints [30–33] (G2M, $p = 1.43 \times 10^{-12}$), Myc targets [34–43] (MYC, $p = 1.66 \times 10^{-11}$), and E2F targets [44–52] (E2F, $p = 1.79 \times 10^{-9}$). y-Axis shows gene symbols, and color codes indicate down- or upregulated genes in blue and red, respectively. The size of each circle indicates the log FC.

Discussion

In this study, we showed how continuous overexpression of miR-125a is required for the potent induction of HSC potential that is initiated by this miR, both in vitro and in vivo. This is in contrast to other examples of stem cell reprogramming, such as the induction of pluripotency in adult cells using Yamanaka factors, where a short expression leads to epigenetic changes that permanently alter the fate of the cell [54,55]. Previous studies have associated long-term miR-125a overexpression with leukemia development [3,7]. We show that HSCs that have been temporarily exposed to miR-125a overexpression do not have detrimental effects associated with excessive proliferation, such as HSC exhaustion and leukemic derailment, and still function normally in serial transplantation experiments. By temporarily overexpressing this miR, we show that it is possible to evoke the beneficial enhanced self-renewal capacity in HSPCs and at the same time prevent leukemia onset associated with chronic miR-125a overexpression.

To gain further molecular insight into the role of miR-125a and how it so potently induces HSC self-renewal, we established the transcriptome of cells in which mir-125a was overexpressed. Our current effort to identify potential miR-125a targets using RNA sequencing complements various previous attempts to identify genes that must be repressed for miR-125a to exert its function in HSCs. These previous attempts have used targeted analyses or unbiased microarray and mass spectrometry approaches. For example, targeted luciferase assays have indicated that Bak1 (BCL2 antagonist/killer 1) is a miR-125a target [56]. Another previously used approach is to filter microarray data for predicted targets obtained from miR-target database TargetScan [3]. As the involvement of a miR can alter protein expression of coding target genes, there have also been attempts to detect differential protein abundance. Mass spectrometry has identified mitogen-activated protein kinase 14 (MAPK14 or p38) and protein tyrosine phosphatase nonreceptor type 1 (Ptpn1) [7]. We also previously identified suppressor

of cytokine signaling 3 (Socs3) and signal transducer and activator of transcription 3 (Stat3) and confirmed their differential expression after mir-125a overexpression by quantitative PCR. We also showed that expression of c-Kit is repressed on HSPCs that overexpress miR-125 [8]. Collectively, a total of six studies have attempted to identify miR-125a targets in normal hematopoiesis, either by handpicking promising candidates or using higher-throughput screening [3,4,7,8,57,58]. Although a direct comparison of the results of these different studies is not straightforward because of the use of different experimental setups and models, it is remarkable that none of the various miR-125a targets appears to be consistently affected in these studies or in this current study, whereas there is a strong consensus on the functional changes that occur in HSCs on miR-125a expression. The fact that little overlap is apparent if these various studies are compared suggests that miR-125a exerts its activity by relatively subtle repression of multiple targets.

We identified novel transcripts to be repressed on miR-125a overexpression, including Gls, which has recently been reported to be an important HSC regulator [16]. We also showed how differentially expressed RNAs, on miR-125a overexpression, only partially overlap with predicted miR-125a targets. In addition, we identified multiple predicted miR-125a targets that are upregulated in HSCs and progenitor cells on overexpression of miR-125a. As mentioned above, miR-125a alters the expression of the cKit receptor, which we use to isolate HSCs. When isolating cells for RNA sequencing, this marker could not be used to purify stem cells. Thus, we isolated a less primitive lineage$^-$Sca1$^+$ population, which also contains a large portion of progenitor cells. Therefore, the identified differentially expressed transcripts can be affected in both HSCs and progenitors or potentially only in one of the two populations. On overexpression of miR-125a, the functional changes, such as enhanced proliferation, become immediately apparent. Our transcriptional analysis used cells isolated 12 weeks after initiation of the perturbation. Thus, the genetic perturbation and resulting phenotypical changes that we report are likely the result of a complex interplay of both direct and indirect targets of the miR. Identifying direct targets of miR-125a will require additional studies that can confirm direct interaction between miR and mRNA sequence. Although it has proven to be challenging to identify critical miR-125a targets that are responsible for the induction of HSC self-renewal, continuous efforts to identify these targets are warranted to reveal the mechanisms underlying the observed phenotype. This will potentially allow us to harness our findings to enhance functionality and expansion of HSCs.

Conflict of interest disclosure

No financial interest/relationships with financial interest relating to the topic of this article have been declared.

Acknowledgments

We thank G. Mesander and J. Teunis for their assistance with cell sorting and panel design for flow cytometry. We thank D. Spierings and R. Arjaans for preparation and sequencing of RNA-seq libraries. We also thank E. Zwart and M. Schubert for assistance with bioinformatic data analysis.

This work was supported by grants from Dutch Organization for Medical Research ZonMW and a TOP grant from the Netherlands Organization for Scientific Research.

References

1. O'Connell RM, Chaudhuri AA, Rao DS, Gibson WSJ. MicroRNAs enriched in hematopoietic stem cells differentially regulate long-term hematopoietic output. Proc Natl Acad Sci USA. 2010;107:14235–14240.
2. Bissels U, Bosio A, Wagner W. MicroRNAs are shaping the hematopoietic landscape. Haematologica. 2012;97:160–167.
3. Gerrits A, Walasek MA, Olthof S, et al. Genetic screen identifies microRNA cluster 99b/let-7e/125a as a regulator of primitive hematopoietic cells. Blood. 2012;119:377–387.
4. Guo S, Lu J, Schlanger R, et al. MicroRNA miR-125a controls hematopoietic stem cell number. Proc Natl Acad Sci USA. 2010;107:14229–14234.
5. Wojtowicz EE, Walasek MA, Broekhuis MJC, et al. MicroRNA-125 family members exert a similar role in the regulation of murine hematopoiesis. Exp Hematol. 2014;42:909–918.
6. Potenza N, Russo A. Biogenesis, evolution and functional targets of microRNA-125a. Mol Genet Genom. 2013;288:381–389.
7. Wojtowicz EE, Lechman ER, Hermans KG, et al. Ectopic miR-125a expression induces long-term repopulating stem cell capacity in mouse and human hematopoietic progenitors. Cell Stem Cell. 2016;19:383–396.
8. Wojtowicz EE, Broekhuis MJC, Weersing E, et al. MiR-125a enhances self-renewal, lifespan, and migration of murine hematopoietic stem and progenitor cell clones. Sci Rep. 2019;9:4785.
9. Silver DP, Livingston DM. Self-excising retroviral vectors encoding the Cre recombinase overcome Cre-mediated cellular toxicity. Mol Cell. 2001;8:233–243.
10. Wilkinson AC, Ishida R, Kikuchi M, et al. Long-term ex vivo haematopoietic-stem-cell expansion allows nonconditioned transplantation. Nature. 2019;571:117–121.
11. Ploemacher RE, Van der Sluijs JP, Van Beurden CAJ, Baert MRM, Chan PL. Use of limiting-dilution type long-term marrow cultures in frequency analysis of marrow-repopulating and spleen colony-forming hematopoietic stem cells in the mouse. Blood. 1991;78:2527–2533.
12. Szilvassy SJ, Weller KP, Lin W, et al. Leukemia inhibitory factor upregulates cytokine expression by a murine stromal cell line enabling the maintenance of highly enriched competitive repopulating stem cells. Blood. 1996;87:4618–4628.
13. Van Os RP, Dethmers-Ausema B, De Haan G. In vitro assays for cobblestone area-forming cells, LTC-IC, and CFU-C. Methods Mol Biol. 2007;430:143–157.

14. Hu Y, Smyth GK. ELDA: extreme limiting dilution analysis for comparing depleted and enriched populations in stem cell and other assays. J Immunol Methods. 2009;347:70–78.
15. Edgar R, Domrachev M, Lash AE. Gene expression omnibus: NCBI gene expression and hybridization array data repository. Nucleic Acids Res. 2002;30:207–210.
16. Sommerkamp P, Altamura S, Renders S, et al. Differential alternative polyadenylation landscapes mediate hematopoietic stem cell activation and regulate glutamine metabolism. Cell Stem Cell. 2020;26:722–738. e7.
17. Li P, Karaczyn AA, McGlauflin R, et al. Novel roles for podocalyxin in regulating stress myelopoiesis, Rap1a, and neutrophil migration. Exp Hematol. 2017;50:77–83.
18. Arai A, Nosaka Y, Kanda E, Yamamoto K, Miyasaka N, Miura O. Rap1 is activated by erythropoietin or interleukin-3 and is involved in regulation of β1 integrin-mediated hematopoietic cell adhesion. J Biol Chem. 2001;276:10453–10462.
19. Minato N. Rap G protein signal in normal and disordered lymphohematopoiesis. Exp Cell Res. 2013;319:2323–2328.
20. Millar AL, Pavlos NJ, Xu J, Zheng MH. Rab3D: a regulator of exocytosis in non-neuronal cells. Histol Histopathol. 2002;17:929–936.
21. Yasunaga M, Saijou S, Hanaoka S, Anzai T, Tsumura R, Matsumura Y. Significant antitumor effect of an antibody against TMEM180, a new colorectal cancer-specific molecule. Cancer Sci. 2019;110:761–770.
22. Anzai T, Matsumura Y. Topological analysis of TMEM180, a newly identified membrane protein that is highly expressed in colorectal cancer cells. Biochem Biophys Res Commun. 2019;520:566–572.
23. Kelwick R, Desanlis I, Wheeler GN, Edwards DR. The ADAMTS (A disintegrin and metalloproteinase with thrombospondin motifs) family. Genome Biol. 2015;16:113.
24. Doyle JM, Gao J, Wang J, Yang M, Potts PR. MAGE–RING protein complexes comprise a family of E3 ubiquitin ligases. Mol Cell. 2010;39:963–974.
25. Chiriaco M, Salfa I, Di Matteo G, Rossi P, Finocchi A. Chronic granulomatous disease: clinical, molecular, and therapeutic aspects. Pediatr Allergy Immunol. 2016;27:242–253.
26. Martino S, Tiribuzi R, Ciraci E, et al. Coordinated involvement of cathepsins S, D and cystatin C in the commitment of hematopoietic stem cells to dendritic cells. Int J Biochem Cell Biol. 2011;43:775–783.
27. Gasiorek JJ, Blank V. Regulation and function of the NFE2 transcription factor in hematopoietic and non-hematopoietic cells. Cell Mol Life Sci. 2015;72:2323–2335.
28. Perez Y, Bar-Yaacov R, Kadir R, et al. Mutations in the microtubule-associated protein MAP11 (C7orf43) cause microcephaly in humans and zebrafish. Brain. 2019;142:574–585.
29. Liberzon A, Birger C, Thorvaldsdóttir H, Ghandi M, Mesirov JP, Tamayo P. The Molecular Signatures Database (MSigDB) hallmark gene set collection. Cell Syst. 2015;1:417–425.
30. Dreij K, Rhrissorrakrai K, Gunsalus KC, Geacintov NE, Scicchitano DA. Benzo[a]pyrene diol epoxide stimulates an inflammatory response in normal human lung fibroblasts through a p53 and JNK mediated pathway. Carcinogenesis. 2010;31:1149–1157.
31. Sadasivam S, Duan S, DeCaprio JA. The MuvB complex sequentially recruits B-Myb and FoxM1 to promote mitotic gene expression. Genes Dev. 2012;26:474–489.
32. Almeida GM, Duarte TL, Farmer PB, Steward WP, Jones GDD. Multiple end-point analysis reveals cisplatin damage tolerance to be a chemoresistance mechanism in a NSCLC model: implications for predictive testing. Int J Cancer. 2008;122:1810–1819.
33. Rashi-Elkeles S, Elkon R, Shavit S, et al. Transcriptional modulation induced by ionizing radiation: P53 remains a central player. Mol Oncol. 2011;5:336–348.
34. Seitz V, Butzhammer P, Hirsch B, et al. Deep sequencing of MYC DNA-binding sites in Burkitt lymphoma. PLoS One. 2011;6:e26837.
35. Rounbehler RJ, Fallahi M, Yang C, et al. Tristetraprolin impairs Myc-induced lymphoma and abolishes the malignant state. Cell. 2012;150:563–574.
36. Ji H, Wu G, Zhan X, et al. Cell-type independent MYC target genes reveal a primordial signature involved in biomass accumulation. PLoS One. 2011;6:e26057.
37. Keller U, Huber J, Nilsson JA, et al. Myc suppression of Nfkb2 accelerates lymphomagenesis. BMC Cancer. 2010;10:348.
38. Nilsson JA, et al. Targeting ornithine decarboxylase in Myc-induced lymphomagenesis prevents tumor formation. Cancer Cell. 2005;7:433–444.
39. Lawlor ER, Soucek L, Brown-Swigart L, Shchors K, Uli Bialucha C, Evan GI. Reversible kinetic analysis of Myc targets in vivo provides novel insights into Myc-mediated tumorigenesis. Cancer Res. 2006;66:4591–4601.
40. Cappellen D, Schlange T, Bauer M, Maurer F, Hynes NE. Novel c-MYC target genes mediate differential effects on cell proliferation and migration. EMBO Rep. 2007;8:70–76.
41. Musgrove EA, Sergio CM, Loi S, et al. Identification of functional networks of estrogen- and c-Myc-responsive genes and their relationship to response to tamoxifen therapy in breast cancer. PLoS One. 2008;3:e2987.
42. Singh P, Alley TL, Wright SM, et al. Global changes in processing of mRNA 3′ untranslated regions characterize clinically distinct cancer subtypes. Cancer Res. 2009;69:9422–9430.
43. Skrzypczak M, Goryca G, Rubel T, et al. Modeling oncogenic signaling in colon tumors by multidirectional analyses of microarray data directed for maximization of analytical reliability. PLoS One. 2010;5:e13091.
44. Chong JL, Wenzel PL, Sáenz-Robles MT, et al. E2f1-3 switch from activators in progenitor cells to repressors in differentiating cells. Nature. 2009;462:930–934.
45. Wenzel PL, Chong JL, Sáenz-Robles MT, et al. Cell proliferation in the absence of E2F1–3. Dev Biol. 2011;351:35–45.
46. Ouseph MM, Li J, Chen HZ, et al. Atypical E2F repressors and activators coordinate placental development. Dev Cell. 2012;22:849–862.
47. Costa C, Santos M, Martinez-Fernández M, et al. E2F1 loss induces spontaneous tumour development in Rb-deficient epidermis. Oncogene. 2013;32:2937–2951.
48. Cecchini MJ, Thwaites MJ, Talluri S, et al. A retinoblastoma allele that is mutated at its common E2F interaction site inhibits cell proliferation in gene-targeted mice. Mol Cell Biol. 2014;34:2029–2045.
49. Hallstrom TC, Mori S, Nevins JR. An E2F1-dependent gene expression program that determines the balance between proliferation and cell death. Cancer Cell. 2008;13:11–22.
50. Maraver A, Fernandez-Marcos PJ, Cash TP, et al. NOTCH pathway inactivation promotes bladder cancer progression. J Clin Invest. 2015;125:824–830.
51. Santos M, Martínez-Fernández M, Dueñas M, et al. In vivo disruption of an Rb-E2F-Ezh2 signaling loop causes bladder cancer. Cancer Res. 2014;74:6565–6577.
52. Lin SH, Beane L, Chasse D, Zhu KW, Mathey-Prevot B, Chang JT. Cross-platform prediction of gene expression signatures. PLoS One. 2013;8:e79228.
53. Miller DM, Thomas SD, Islam A, Muench D, Sedoris K. c-Myc and cancer metabolism. Clin Cancer Res. 2012;18:5546–5553.

54. Takahashi K, Yamanaka S. Induction of pluripotent stem cells from mouse embryonic and adult fibroblast cultures by defined factors. Cell. 2006;126:663–676.
55. Takahashi K, Tanabe K, Ohnuki M, et al. Induction of pluripotent stem cells from adult human fibroblasts by defined factors. Cell. 2007;131:861–872.
56. Guo S, Scadden DT. A microRNA regulating adult hematopoietic stem cells. Cell Cycle. 2010;9:3637–3638.
57. Chaudhuri AA, So AY, Mehta A, et al. Oncomir miR-125b regulates hematopoiesis by targeting the gene Lin28A. Proc Natl Acad Sci USA. 2012;109:4233–4238.
58. Ooi AGL, Sahoo D, Adorno M, Wang Y, Weissman IL, Park CY. MicroRNA-125b expands hematopoietic stem cells and enriches for the lymphoid-balanced and lymphoid-biased subsets. Proc Natl Acad ScI USA. 2010;107:21505–21510.

Appendix. Supplementary materials

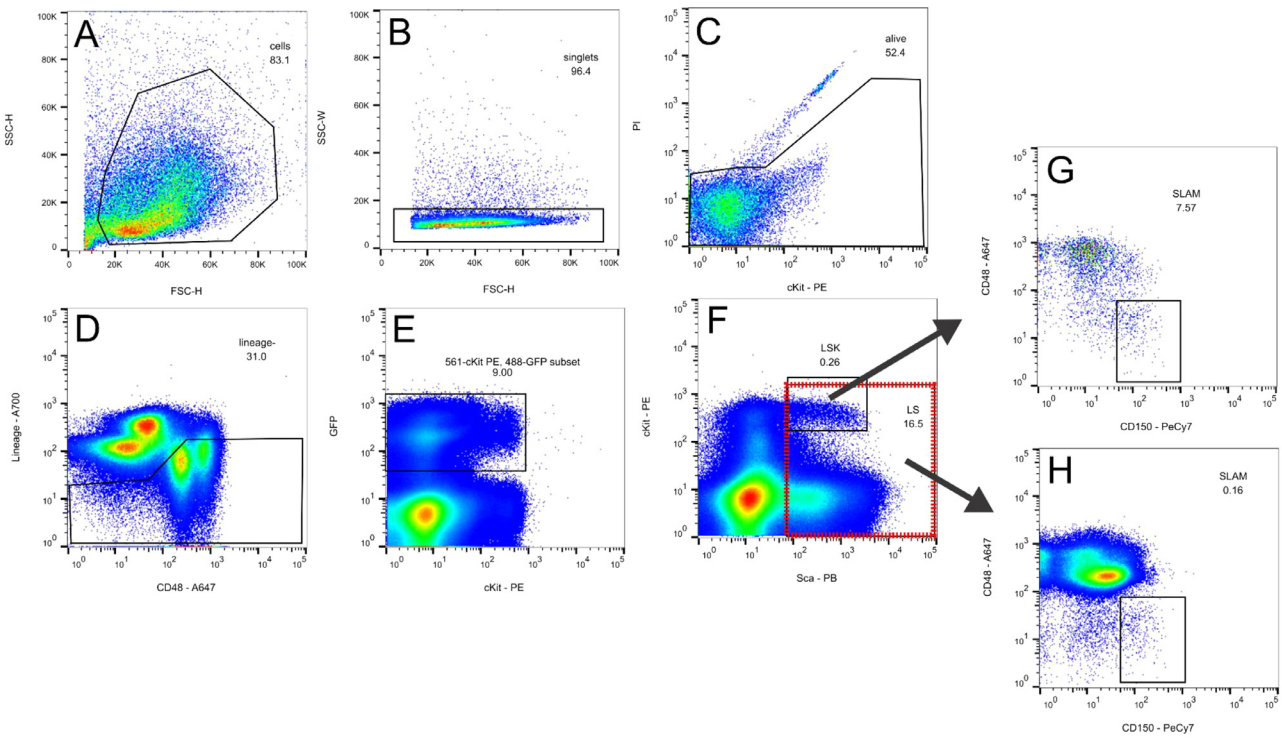

Figure E1. Sorting strategy for bone marrow of primary recipients, gate marked in red dashed line indicates sorting gate. Hierarchy of gates according to alphabetical order of panels. (A) Cells, SSC-H vs FSC-H (B) Singlets, SSC-W vs. FSC-H. (C) Living cells, PI vs. cKit-PE. (D) Lineage negative, lineage-A700 vs. CD48-A647. (E) GFP positive cells, GFP vs. cKit-PE. (F) Sorting gate LS, HSC gate LSK, cKit-PE vs. Sca1-PB. (G and H) HSC compartment LSK/SLAM of LSK compartment in G and of sorted LS compartment in H. CD48-A647 vs. CD150-PE-Cy7.

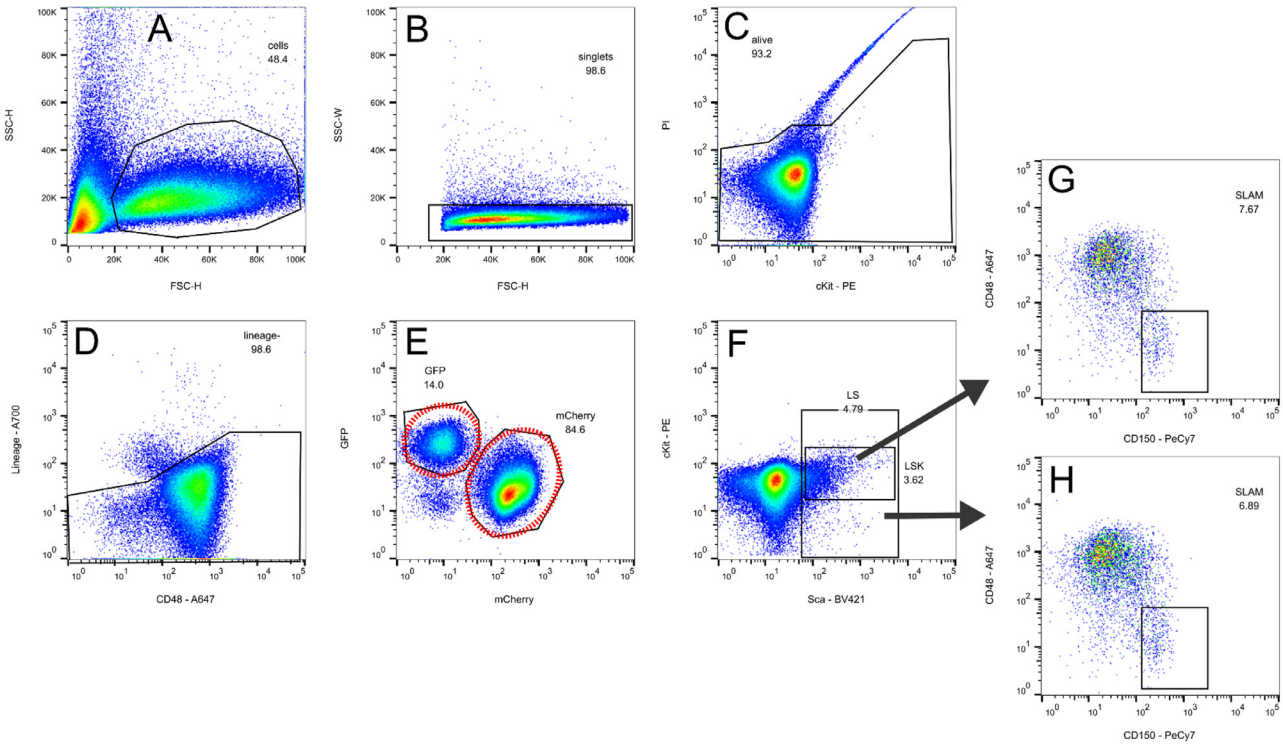

Figure E2. Sorting strategy of in-vitro expanded cells, gate marked in panel E with red dashed line indicates sorting gate for separation of GFP + and mCherry+ cells. Hierarchy of gates according to alphabetical order of panels. (A) Cells, SSC-H vs FSC-H (B) Singlets, SSC-W vs. FSC-H. (C) Living cells, PI vs. cKit-PE. (D) Lineage negative, lineage-A700 vs. CD48-A647. (E) GFP positive cells, GFP vs. cKit-PE. (F) Sorting gate LS, HSC gate LSK, cKit-PE vs. Sca1-PB. (G and H) HSC compartment LSK/SLAM of LSK compartment in G and of sorted LS compartment in H. CD48-A647 vs. CD150-PE-Cy7.

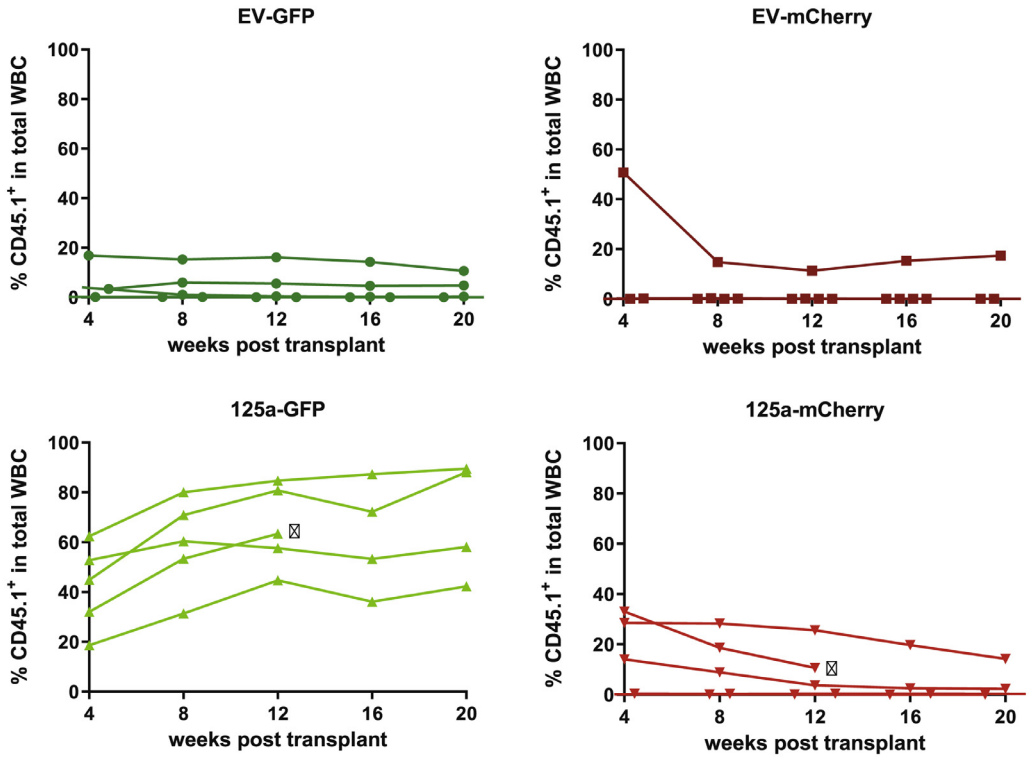

Figure E3. Engraftment of donor cells per mouse (n=5). Showing contribution of CD45.1+ donor cells to the recipient peripheral blood at 4-week intervals as a representation of donor cell engraftment. Each line represents consecutive sampling of the same recipient, each panel represents an experimental group. Experimental set up as shown in Fig. 4 and 5.

Table S1. Differential expression Top 100

	Row.names	ensembl_gene_id_version	ensembl_gene_id	external_gene_name	logFC	logCPM	LR	PValue	FDR
1	ENSMUSG00000000253.13	ENSMUSG00000000253.13	ENSMUSG00000000253	Gmpr	-2.56976	5.122974	11.94154	0.000549	0.029921
2	ENSMUSG00000000326.13	ENSMUSG00000000326.13	ENSMUSG00000000326	Comt	3.364178	5.624679	15.25819	9.38E-05	0.009863
3	ENSMUSG00000001403.13	ENSMUSG00000001403.13	ENSMUSG00000001403	Ube2c	4.517271	6.383617	17.69014	2.60E-05	0.004474
4	ENSMUSG00000001918.17	ENSMUSG00000001918.17	ENSMUSG00000001918	Slc1a5	3.027827	5.848358	11.85702	0.000574	0.03054
5	ENSMUSG00000002014.12	ENSMUSG00000002014.12	ENSMUSG00000002014	Ssr4	2.904996	5.2756	13.45214	0.000245	0.01813
6	ENSMUSG00000002043.17	ENSMUSG00000002043.17	ENSMUSG00000002043	Trappc6a	-3.54182	5.906463	15.06383	0.000104	0.010365
7	ENSMUSG00000002222.14	ENSMUSG00000002222.14	ENSMUSG00000002222	Rmnd5a	3.382292	5.166205	17.58639	2.75E-05	0.004586
8	ENSMUSG00000002289.16	ENSMUSG00000002289.16	ENSMUSG00000002289	Angptl4	-5.31486	6.954562	19.2903	1.12E-05	0.002989
9	ENSMUSG00000002997.15	ENSMUSG00000002997.15	ENSMUSG00000002997	Prkar2b	2.331427	4.796692	10.78896	0.001021	0.044725
10	ENSMUSG00000004268.11	ENSMUSG00000004268.11	ENSMUSG00000004268	Emg1	5.074319	6.903899	18.13886	2.05E-05	0.004037
11	ENSMUSG00000004285.12	ENSMUSG00000004285.12	ENSMUSG00000004285	Atp6v1f	-3.09793	5.774917	12.81765	0.000343	0.022589
12	ENSMUSG00000004552.16	ENSMUSG00000004552.16	ENSMUSG00000004552	Ctse	4.628821	8.686573	13.49583	0.000239	0.01779
13	ENSMUSG00000004642.13	ENSMUSG00000004642.13	ENSMUSG00000004642	Slbp	4.581331	7.285043	14.63933	0.00013	0.012187
14	ENSMUSG00000004936.8	ENSMUSG00000004936.8	ENSMUSG00000004936	Map2k1	-3.67267	5.915472	15.8532	6.85E-05	0.008156
15	ENSMUSG00000005262.13	ENSMUSG00000005262.13	ENSMUSG00000005262	Ufd1	3.186031	5.509847	14.52268	0.000138	0.012537
16	ENSMUSG00000005686.17	ENSMUSG00000005686.17	ENSMUSG00000005686	Ampd3	2.752238	5.578462	11.29276	0.000778	0.03683
17	ENSMUSG00000005800.3	ENSMUSG00000005800.3	ENSMUSG00000005800	Mmp8	5.128545	8.454639	15.91077	6.64E-05	0.008027
18	ENSMUSG00000006005.18	ENSMUSG00000006005.18	ENSMUSG00000006005	Tpr	4.568617	7.724853	13.97183	0.000186	0.015155
19	ENSMUSG00000006021.5	ENSMUSG00000006021.5	ENSMUSG00000006021	Kptn	3.08415	4.732311	16.46528	4.95E-05	0.006809
20	ENSMUSG00000006127.9	ENSMUSG00000006127.9	ENSMUSG00000006127	Inpp5k	5.555839	7.504147	18.62645	1.59E-05	0.003612
21	ENSMUSG00000006299.13	ENSMUSG00000006299.13	ENSMUSG00000006299	Aamp	-3.19162	5.451337	15.05195	0.000105	0.010365
22	ENSMUSG00000006398.15	ENSMUSG00000006398.15	ENSMUSG00000006398	Cdc20	-2.42574	3.923452	10.90473	0.000959	0.0432
23	ENSMUSG00000006403.13	ENSMUSG00000006403.13	ENSMUSG00000006403	Adamts4	-3.75132	6.868782	11.76942	0.000602	0.030902
24	ENSMUSG00000007817.15	ENSMUSG00000007817.15	ENSMUSG00000007817	Zmiz1	-3.31594	6.256595	11.73133	0.000615	0.031165
25	ENSMUSG00000007836.6	ENSMUSG00000007836.6	ENSMUSG00000007836	Hnrnpa0	2.90763	5.260367	13.57197	0.00023	0.017264
26	ENSMUSG00000007891.16	ENSMUSG00000007891.16	ENSMUSG00000007891	Ctsd	-3.00568	4.714735	16.50139	4.86E-05	0.006734
27	ENSMUSG00000008976.16	ENSMUSG00000008976.16	ENSMUSG00000008976	Gabpa	4.273315	7.423121	12.84512	0.000338	0.022499
28	ENSMUSG00000009079.16	ENSMUSG00000009079.16	ENSMUSG00000009079	Ewsr1	3.678235	6.497295	12.58532	0.000389	0.024719
29	ENSMUSG00000009549.14	ENSMUSG00000009549.14	ENSMUSG00000009549	Srp14	-2.60536	5.404046	10.98503	0.000919	0.041846
30	ENSMUSG00000009585.18	ENSMUSG00000009585.18	ENSMUSG00000009585	Apobec3	2.923845	5.429192	12.96862	0.000317	0.021675
31	ENSMUSG00000010376.15	ENSMUSG00000010376.15	ENSMUSG00000010376	Nedd8	4.143289	6.157042	17.01402	3.71E-05	0.005645
32	ENSMUSG00000012422.14	ENSMUSG00000012422.14	ENSMUSG00000012422	Tmem167	3.021044	5.913457	11.57214	0.000669	0.033064
33	ENSMUSG00000013974.3	ENSMUSG00000013974.3	ENSMUSG00000013974	Mcemp1	2.602747	4.882572	12.64846	0.000376	0.024168
34	ENSMUSG00000014232.14	ENSMUSG00000014232.14	ENSMUSG00000014232	Cluap1	5.214023	7.16671	17.96113	2.25E-05	0.004131
35	ENSMUSG00000014769.10	ENSMUSG00000014769.10	ENSMUSG00000014769	Psmb1	-5.50447	7.731819	18.29616	1.89E-05	0.003978
36	ENSMUSG00000014956.15	ENSMUSG00000014956.15	ENSMUSG00000014956	Ppp1cb	3.540032	4.929777	19.53032	9.90E-06	0.002798
37	ENSMUSG00000015656.17	ENSMUSG00000015656.17	ENSMUSG00000015656	Hspa8	-3.46533	6.322586	12.32246	0.000448	0.02733
38	ENSMUSG00000015950.13	ENSMUSG00000015950.13	ENSMUSG00000015950	Ncf1	-3.28966	4.944598	18.29817	1.89E-05	0.003978
39	ENSMUSG00000016554.9	ENSMUSG00000016554.9	ENSMUSG00000016554	Eif3d	-2.7833	5.513662	11.89089	0.000564	0.030233
40	ENSMUSG00000017404.12	ENSMUSG00000017404.12	ENSMUSG00000017404	Rpl19	-2.99025	5.568649	13.1968	0.00028	0.019909
41	ENSMUSG00000017428.16	ENSMUSG00000017428.16	ENSMUSG00000017428	Psmd11	2.777916	5.410618	12.03436	0.000522	0.029468
42	ENSMUSG00000017778.14	ENSMUSG00000017778.14	ENSMUSG00000017778	Cox7c	3.027704	4.214092	15.77697	7.13E-05	0.008374
43	ENSMUSG00000018326.9	ENSMUSG00000018326.9	ENSMUSG00000018326	Ywhab	-3.10999	6.014443	11.75549	0.000607	0.031041
44	ENSMUSG00000018362.14	ENSMUSG00000018362.14	ENSMUSG00000018362	Kpna2	3.352939	5.495474	15.69906	7.43E-05	0.008608
45	ENSMUSG00000018433.14	ENSMUSG00000018433.14	ENSMUSG00000018433	Nol11	6.942534	9.157916	23.50463	1.25E-06	0.000786
46	ENSMUSG00000018476.7	ENSMUSG00000018476.7	ENSMUSG00000018476	Kdm6b	-3.62049	7.005774	10.79055	0.00102	0.044725
47	ENSMUSG00000019066.13	ENSMUSG00000019066.13	ENSMUSG00000019066	Rab3d	-4.7109	7.470983	14.85037	0.000116	0.011115
48	ENSMUSG00000019082.18	ENSMUSG00000019082.18	ENSMUSG00000019082	Slc25a22	-3.11249	6.131281	11.15028	0.00084	0.039115
49	ENSMUSG00000019505.7	ENSMUSG00000019505.7	ENSMUSG00000019505	Ubb	5.833651	6.337674	24.54974	7.24E-07	0.000561
50	ENSMUSG00000019528.18	ENSMUSG00000019528.18	ENSMUSG00000019528	Gyg	5.129065	8.176846	16.14625	5.86E-05	0.007569

Table S1. (*Continued*)

51	ENSMUSG00000019774.8	ENSMUSG00000019774.8	ENSMUSG00000019774	Mtrf1l	4.233033	6.549967	15.31623	9.09E-05	0.009684
52	ENSMUSG00000019795.17	ENSMUSG00000019795.17	ENSMUSG00000019795	Pcmt1	4.79954	6.471668	18.6912	1.54E-05	0.003587
53	ENSMUSG00000019872.13	ENSMUSG00000019872.13	ENSMUSG00000019872	Smpdl3a	-3.29625	5.462301	15.93103	6.57E-05	0.008027
54	ENSMUSG00000019942.13	ENSMUSG00000019942.13	ENSMUSG00000019942	Cdk1	5.450925	7.251382	18.76507	1.48E-05	0.003548
55	ENSMUSG00000020076.7	ENSMUSG00000020076.7	ENSMUSG00000020076	Ddx50	-5.09289	8.305797	15.96225	6.46E-05	0.008027
56	ENSMUSG00000020248.18	ENSMUSG00000020248.18	ENSMUSG00000020248	Nfyb	3.93714	8.058713	10.87946	0.000972	0.043486
57	ENSMUSG00000020267.6	ENSMUSG00000020267.6	ENSMUSG00000020267	Hint1	5.627275	4.821478	32.05087	1.50E-08	4.11E-05
58	ENSMUSG00000020290.14	ENSMUSG00000020290.14	ENSMUSG00000020290	Xpo1	3.057006	6.02051	11.2747	0.000786	0.036881
59	ENSMUSG00000020372.15	ENSMUSG00000020372.15	ENSMUSG00000020372	Rack1	5.44173	7.419811	18.20087	1.99E-05	0.004037
60	ENSMUSG00000020496.9	ENSMUSG00000020496.9	ENSMUSG00000020496	Rnf187	-4.78229	8.30826	14.51448	0.000139	0.012537
61	ENSMUSG00000020570.15	ENSMUSG00000020570.15	ENSMUSG00000020570	Sypl	6.45985	8.948173	21.34579	3.83E-06	0.001719
62	ENSMUSG00000020585.4	ENSMUSG00000020585.4	ENSMUSG00000020585	Laptm4a	2.797151	5.584919	11.60744	0.000657	0.032727
63	ENSMUSG00000020612.16	ENSMUSG00000020612.16	ENSMUSG00000020612	Prkar1a	-5.88058	8.226044	19.61433	9.48E-06	0.002798
64	ENSMUSG00000020671.9	ENSMUSG00000020671.9	ENSMUSG00000020671	Rab10	2.67467	5.491943	11.09915	0.000864	0.039907
65	ENSMUSG00000020719.14	ENSMUSG00000020719.14	ENSMUSG00000020719	Ddx5	4.344758	8.512894	12.35282	0.00044	0.027085
66	ENSMUSG00000020994.5	ENSMUSG00000020994.5	ENSMUSG00000020994	Pnn	3.271015	4.918751	17.60175	2.72E-05	0.004586
67	ENSMUSG00000021018.8	ENSMUSG00000021018.8	ENSMUSG00000021018	Polr2h	-4.70785	6.155141	20.61629	5.61E-06	0.002191
68	ENSMUSG00000021131.14	ENSMUSG00000021131.14	ENSMUSG00000021131	Erh	2.860199	4.111793	13.96863	0.000186	0.015155
69	ENSMUSG00000021248.9	ENSMUSG00000021248.9	ENSMUSG00000021248	Tmed10	-5.44032	6.845984	20.36524	6.40E-06	0.002368
70	ENSMUSG00000021250.13	ENSMUSG00000021250.13	ENSMUSG00000021250	Fos	5.641339	4.843191	31.82345	1.69E-08	4.11E-05
71	ENSMUSG00000021256.5	ENSMUSG00000021256.5	ENSMUSG00000021256	Vash1	-3.10895	6.095166	11.27952	0.000784	0.036881
72	ENSMUSG00000021610.8	ENSMUSG00000021610.8	ENSMUSG00000021610	Clptm1l	-4.29841	6.994236	14.195	0.000165	0.013971
73	ENSMUSG00000021615.13	ENSMUSG00000021615.13	ENSMUSG00000021615	Xrcc4	2.468389	4.617784	11.97207	0.00054	0.029921
74	ENSMUSG00000021619.6	ENSMUSG00000021619.6	ENSMUSG00000021619	Atg10	2.481658	4.277041	11.93333	0.000551	0.029921
75	ENSMUSG00000021645.16	ENSMUSG00000021645.16	ENSMUSG00000021645	Smn1	-2.55428	3.959854	12.19669	0.000479	0.028542
76	ENSMUSG00000021646.9	ENSMUSG00000021646.9	ENSMUSG00000021646	Mccc2	4.360662	6.516053	16.1613	5.82E-05	0.007569
77	ENSMUSG00000021748.9	ENSMUSG00000021748.9	ENSMUSG00000021748	Pdhb	5.213588	7.0496	18.3021	1.88E-05	0.003978
78	ENSMUSG00000021771.14	ENSMUSG00000021771.14	ENSMUSG00000021771	Vdac2	3.003587	5.4431	13.56865	0.00023	0.017264
79	ENSMUSG00000021891.8	ENSMUSG00000021891.8	ENSMUSG00000021891	Mettl6	4.499163	8.644732	12.94515	0.000321	0.021861
80	ENSMUSG00000021973.9	ENSMUSG00000021973.9	ENSMUSG00000021973	Micu2	3.215095	4.368098	17.31285	3.17E-05	0.005049
81	ENSMUSG00000022009.1	ENSMUSG00000022009.1	ENSMUSG00000022009	Nufip1	5.324599	7.689977	17.44484	2.96E-05	0.004877
82	ENSMUSG00000022043.19	ENSMUSG00000022043.19	ENSMUSG00000022043	Trim35	-3.52119	6.29961	12.74704	0.000357	0.023161
83	ENSMUSG00000022216.17	ENSMUSG00000022216.17	ENSMUSG00000022216	Psme1	2.718558	4.667047	13.64178	0.000221	0.016902
84	ENSMUSG00000022601.11	ENSMUSG00000022601.11	ENSMUSG00000022601	Zbtb11	3.627001	6.744473	11.43264	0.000722	0.035032
85	ENSMUSG00000022969.13	ENSMUSG00000022969.13	ENSMUSG00000022969	Il10rb	-5.32159	7.322472	18.15339	2.04E-05	0.004037
86	ENSMUSG00000023048.13	ENSMUSG00000023048.13	ENSMUSG00000023048	Prr13	-4.4609	6.697935	15.94327	6.53E-05	0.008027
87	ENSMUSG00000024012.18	ENSMUSG00000024012.18	ENSMUSG00000024012	Mtch1	2.322459	4.70587	10.66637	0.001091	0.046944
88	ENSMUSG00000024072.9	ENSMUSG00000024072.9	ENSMUSG00000024072	Yipf4	2.766546	5.366732	12.08645	0.000508	0.029097
89	ENSMUSG00000024097.11	ENSMUSG00000024097.11	ENSMUSG00000024097	Srsf7	5.034655	8.168518	15.72212	7.34E-05	0.008562
90	ENSMUSG00000024098.6	ENSMUSG00000024098.6	ENSMUSG00000024098	Twsg1	3.599143	5.176464	18.89214	1.38E-05	0.003409
91	ENSMUSG00000024300.17	ENSMUSG00000024300.17	ENSMUSG00000024300	Myo1f	-5.10591	6.968488	18.18684	2.00E-05	0.004037
92	ENSMUSG00000024521.8	ENSMUSG00000024521.8	ENSMUSG00000024521	Pmaip1	-3.00473	5.165681	15.04029	0.000105	0.010365
93	ENSMUSG00000024580.8	ENSMUSG00000024580.8	ENSMUSG00000024580	Grpel2	-3.76244	6.854166	11.87941	0.000568	0.030317
94	ENSMUSG00000024673.9	ENSMUSG00000024673.9	ENSMUSG00000024673	Ms4a1	2.874683	5.839445	10.9448	0.000939	0.04265
95	ENSMUSG00000024681.11	ENSMUSG00000024681.11	ENSMUSG00000024681	Ms4a3	-2.54162	5.161682	11.40838	0.000731	0.035092
96	ENSMUSG00000024687.11	ENSMUSG00000024687.11	ENSMUSG00000024687	Osbp	-3.54998	6.31864	12.76132	0.000354	0.023101
97	ENSMUSG00000024795.11	ENSMUSG00000024795.11	ENSMUSG00000024795	Kif20b	4.663474	8.399912	13.86884	0.000196	0.015681
98	ENSMUSG00000024845.17	ENSMUSG00000024845.17	ENSMUSG00000024845	Tmem134	3.445138	5.045258	18.56241	1.64E-05	0.003686
99	ENSMUSG00000024976.14	ENSMUSG00000024976.14	ENSMUSG00000024976	Shoc2	5.512023	7.119598	19.47713	1.02E-05	0.002798
100	ENSMUSG00000024991.8	ENSMUSG00000024991.8	ENSMUSG00000024991	Eif3a	4.004857	7.199683	12.15167	0.00049	0.028816

Table S2. Overlap analysis gene sets

Overlap UP+DOWN Hallmarks (https://www.gsea-msigdb.org/) 28-07-2020						
Overlap Results						
Collection(s):	H					
# overlaps shown:	10					
# genesets in collections:	50					
# genes in comparison (n):	321					
# genes in universe (N):	38404					
Gene Set Name	# Genes in Gene Set (K)	Description	# Genes in Overlap (k)	k/K	p-value	FDR q-value
HALLMARK_G2M_CHECKPOINT	200	Genes involved in the G2/M checkpoi	17	0.085	1.43E-12	7.17E-11
HALLMARK_MYC_TARGETS_V1	200	A subgroup of genes regulated by MY	16	0.08	1.66E-11	4.14E-10
HALLMARK_E2F_TARGETS	200	Genes encoding cell cycle related tar	14	0.07	1.79E-09	2.99E-08
HALLMARK_UV_RESPONSE_UP	158	Genes up-regulated in response to ul	10	0.0633	9.71E-07	1.12E-05
HALLMARK_OXIDATIVE_PHOSPHORY	200	Genes encoding proteins involved in	11	0.055	1.12E-06	1.12E-05
HALLMARK_MITOTIC_SPINDLE	199	Genes important for mitotic spindle a	10	0.0503	7.67E-06	4.46E-05
HALLMARK_GLYCOLYSIS	200	Genes encoding proteins involved in	10	0.05	8.02E-06	4.46E-05
HALLMARK_HYPOXIA	200	Genes up-regulated in response to lo	10	0.05	8.02E-06	4.46E-05
HALLMARK_MTORC1_SIGNALING	200	Genes up-regulated through activatic	10	0.05	8.02E-06	4.46E-05
HALLMARK_COMPLEMENT	200	Genes encoding components of the c	9	0.045	5.19E-05	2.54E-04